

ADVANCED OPTICS LAB - ECEN 5606

Kelvin Wagner

Experiment No. 13

ACOUSTOOPTIC DEVICES

September 17, 2001

1 Introduction

In this lab you will learn to use acoustooptic modulators and deflectors in order to manipulate the intensity, frequency, and direction of propagation of laser wavefronts. You will optimize the operation of an acoustooptic modulator for large diffraction efficiency, and wide modulation bandwidth, and you will learn the difference between modulators and deflectors. This writeup gives a comprehensive review of the conventional treatment of the mathematics and physics describing optical and acoustic wave and the acousto-optic interaction, as well as the operation of modulator and deflector devices. Then in the appendix, the formal derivation of the graphical approach to describing acousto-optics based on momentum space is presented.

2 Background

Acoustooptic devices are based on the periodic modulation of the optical index of refraction caused by an acoustic wave propagating in a transparent material. An optical wave passing through the region containing the acoustic wave will experience a periodic phase modulation that can produce a corrugation of the optical wavefront which will result in a scattering of the optical wave into diffracted orders. The acousto-optic interaction is somewhat different from other types of optical volume diffraction effects because the perturbation is required to be a superposition of propagating eigenmodes of the acoustic wave equation.

The acousto-optic interaction results in the phase modulation of an optical beam by an acoustic wave in a photoelastic medium. In order to properly describe this interaction the acoustic and optical waves will be represented separately, and then the coupling between them will be introduced. This interaction is mediated by the 4th rank photoelastic tensor which describes the dielectric impermeability tensor perturbation caused by the propagating strain wave. In practice, devices are designed to make use of only a single element of the coupling tensor, and the problem is greatly simplified.

2.1 Acoustic eigenmodes

The acoustic wave is modelled as a time and space varying particle displacement vector field $\vec{u}(\vec{x}, t)$, which at each crystal lattice site describes the particle displacement from its equilibrium position[1, 2]. A sinusoidal displacement wave of amplitude W , radian frequency Ω , wave vector

$|\vec{K}| = 2\pi/\Lambda$, acoustic wavelength Λ , propagating with a phase velocity $v_a(\vec{s}) = \Omega/|K|$ in the direction defined by the unit vector $\vec{s} = \vec{K}/|K|$, and with unit polarization \hat{U} is described by the particle displacement field

$$\vec{u}(\vec{x}, t) = W\hat{U} \cos(\Omega t - \vec{K} \cdot \vec{x}) = W\hat{U} \cos \left[\Omega \left(t - \frac{\vec{s} \cdot \vec{x}}{v_a(\vec{s})} \right) \right] \quad (1)$$

The displacement gradient matrix is the spatial derivative of the displacement field, and its components are given by

$$Q_{ij}(\vec{x}, t) = \left[\frac{\partial u_i(\vec{x}, t)}{\partial x_j} \right] \quad (2)$$

The symmetric part of the displacement gradient matrix is known as the linearized Strain tensor and its components are given by

$$\mathbf{S}_{ij} = \frac{1}{2} \left[\frac{\partial u_i}{\partial x_j} + \frac{\partial u_j}{\partial x_i} \right] \quad (3)$$

The Stress tensor \mathbf{T}_{ij} , which is symmetric in non ferroic materials, is related to the Strain tensor through the 4th rank elastic stiffness tensor in a generalization of Hooke's law.

$$\mathbf{T}_{ij} = \mathbf{c}_{ijkl} \mathbf{S}_{kl} \quad (4)$$

Where the Einstein summation convention over repeated indices is implied, and i, j, k, l may take on any of the three spatial directions x_1, x_2, x_3 or equivalently x, y, z . The elastic coefficients possess certain symmetries because of the symmetry of \mathbf{S} and \mathbf{T} , so that $\mathbf{c}_{ijkl} = \mathbf{c}_{jikl} = \mathbf{c}_{ijlk} = \mathbf{c}_{jilk}$, and energy arguments show that $\mathbf{c}_{ijkl} = \mathbf{c}_{klij}$. The acoustic field equations show that energy oscillates between the stress energy and the strain energy in a fashion that is analogous to the electromagnetic oscillation between electric and magnetic energy. The dynamical equation of motion for a vibrating medium relates the restoring force as given by the divergence of the Stress tensor with the mass times acceleration of the displacement field.

$$\vec{F} = \nabla \cdot \mathbf{T} = \rho_m \frac{\partial^2 \vec{u}}{\partial t^2} \quad (5)$$

$$F_i = \frac{\partial}{\partial x_j} \mathbf{T}_{ij} = \rho_m \frac{\partial^2 u_i}{\partial t^2} \quad (6)$$

In this equation ρ_m is the scalar equilibrium mass density of the medium. Substitution of the Stress-Strain relationship, and the definition of Stress in terms of particle displacements into the dynamical equation of motion results in the differential equation governing the propagation of particle displacement fields.

$$F_i = \mathbf{c}_{ijkl} \frac{\partial^2 u_k}{\partial x_l \partial x_j} = \rho_m \frac{\partial^2 u_i}{\partial t^2} \quad (7)$$

Substitution of the assumed plane wave of Equation 1 into this equation results in the equation for the allowed modes of propagation.

$$\mathbf{c}_{ijkl} s_j s_l k^2 U_k = \Gamma_{ik}(\vec{s}) k^2 U_k = \rho_m \Omega^2 U_i \quad (8)$$

$$\left[\mathbf{c}_{ijkl} s_j s_l / v_a^2 - \rho_m \delta_{ik} \right] U_k = 0 \quad (9)$$

This system is only compatible for all waves if the determinant of the system is zero, which results in the dispersion relationship in terms of the Christoffel matrix $\Gamma_{ik}(\vec{s}) = \mathbf{c}_{ijkl}s_js_l$ as a function of the propagation direction \vec{s} , where s_x, s_y, s_z are the appropriate direction cosines.

$$\det \left| \frac{\Gamma_{ik}(\vec{s})}{v_a^2} - \rho_m \delta_{ik} \right| = 0 \quad (10)$$

This equation has three solutions for the acoustic slowness, or inverse velocity $1/v_a(\vec{s}) = \vec{K}/\Omega$ for each direction \vec{s} , forming three equivalent frequency scaled surfaces in \vec{K} space, known as acoustic momentum space. The corresponding eigen-polarizations $\hat{U}(\vec{s})$ for each direction of propagation correspond to the longitudinal (or quasilongitudinal) and two shear (or quasishear) solutions.

2.2 Optical eigenmodes

Optical propagation through a homogenous, lossless anisotropic medium can be described in terms of Maxwell's equations.[3] Faraday's law gives the relation between an induced electric field and a time varying magnetic field. Ampère's law describes the creation of a magnetic field due to a dielectric flux, a conductivity current, and a source current, however for the case of interest to acousto-optics, no currents are present. Similarly, we will assume no free electric charges, and of course no free magnetic monopoles.

$$\nabla \times \vec{E} = -\frac{\partial \vec{B}}{\partial t} \quad (11)$$

$$\nabla \times \vec{H} = \frac{\partial \vec{D}}{\partial t} + \vec{J}_c + \vec{J}_s = \frac{\partial \vec{D}}{\partial t} \quad (12)$$

$$\nabla \cdot \vec{D} = \rho_e = 0 \quad (13)$$

$$\nabla \cdot \vec{B} = 0 \quad (14)$$

In an optically anisotropic medium the displacement vector \vec{D} and electric field \vec{E} are not necessarily parallel, and are related by the Hermitian second rank permittivity tensor ϵ . In magnetically isotropic material the magnetic vector \vec{H} is related to the magnetic induction \vec{B} by the scalar permeability μ . The resulting constitutive relationships describe the effect of material media on the propagation of electromagnetic waves, and allows the unique solution to Maxwell's equations with a given set of boundary conditions.

$$\vec{D} = \epsilon \vec{E} = \epsilon_0 \vec{E} + \vec{P} \quad (15)$$

$$D_i = \epsilon_{ij} E_j = \epsilon_0 (\delta_{ij} + \chi_{ij}) E_j = \epsilon_0 E_i + \chi_{ij} E_j = \epsilon_0 E_i + P_i \quad (16)$$

$$\vec{B} = \mu \vec{H} = \mu_0 \vec{H} + \vec{M} \quad (17)$$

$$B_i = \mu H_i \quad (18)$$

The permittivity tensor is expressed as the free space permittivity ϵ_0 plus a material dependent susceptibility tensor, $\epsilon_{ij} = \epsilon_0(1 + \chi_{ij})$, and the presence of the matter is seen to induce a polarization vector \vec{P} which is related to \vec{E} through the linear susceptibility tensor χ_{ij} .

In order to derive the optical eigenmodes we will assume an electromagnetic plane wave with angular frequency ω , and wave vector $|\vec{k}| = 2\pi/\lambda$, propagating in the direction of the unit vector $\vec{s} = \vec{k}/|\vec{k}|$, with a phase velocity $v_p = c/n = 1/\sqrt{\mu\epsilon}$. The refractive index $n = \sqrt{\epsilon/\epsilon_0}$ is a function

of the direction of propagation, the polarization of the wave, and the frequency if the material is dispersive, and it is the allowed eigen-velocities v_p and eigen-polarizations \vec{E}_0 which are to be determined.

$$\vec{E}(\vec{x}, t) = \vec{E}_0 e^{-i(\omega t - \vec{k} \cdot \vec{x})} \quad (19)$$

$$\vec{H}(\vec{x}, t) = \vec{H}_0 e^{-i(\omega t - \vec{k} \cdot \vec{x})} \quad (20)$$

We can now substitute these assumed solutions into Maxwell's equations to obtain

$$\vec{k} \times \vec{E} = \omega \mu \vec{H} \quad (21)$$

$$\vec{k} \times \vec{H} = -\omega \epsilon \vec{E} \quad (22)$$

Substituting the first equation for \vec{H} into the second equation yields an equation for \vec{E} .

$$\vec{k} \times (\vec{k} \times \vec{E}) + \omega^2 \mu \epsilon \vec{E} = 0 \quad (23)$$

$$\left[k_i k_j - \delta_{ij} k^2 + \omega \mu \epsilon_{ij} \right] E_j = 0 \quad (24)$$

In the absence of optical activity, the symmetry of the permittivity tensor ϵ allows us to rotate to a principal dielectric coordinate system where ϵ_{ij} is purely diagonal. In order for a nontrivial solution to exist the determinant of the matrix in brackets in equation (17b) must be zero.

$$\det \left[k_i k_j - \delta_{ij} k^2 + \omega \mu \epsilon_{ij} \right] = 0 \quad (25)$$

This is the equation for the optical normal surface in \vec{k} space, referred to as optical momentum space. It is analogous to the acoustic momentum surface, and the inverse optical phase velocity $v_p^{-1} = n/c = k/\omega$ in a particular direction, is proportional to the radius of the momentum surface in that direction divided by the optical angular frequency. For each direction of propagation there are two possible eigen-phase-velocities, with corresponding orthogonal, eigen-polarizations as solutions to equation (17). The two surfaces intersect in degenerate directions known as the optical axes, and there may be up to four such intersections in biaxial media, which lie along two optical axes in the xz plane. For uniaxial materials there are only two such intersections along a single line, giving a single optical axis.

The impermeability tensor $\eta_{ij} = \epsilon_0 (\epsilon^{-1})_{ij}$ is the inverse of the dielectric tensor ϵ and is given by the relation $(\epsilon^{-1})_{kj} \epsilon_{ik} = \delta_{ij}$. As a second rank symmetric tensor it describes a quadratic surface known as the index ellipsoid

$$(\epsilon^{-1})_{ij} x_i x_j = \left(\frac{1}{n^2} \right)_{ij} x_i x_j = 1. \quad (26)$$

In the principal coordinate system this equation reduces to the familiar representation of a general ellipsoid.

$$\frac{x_1^2}{n_1^2} + \frac{x_2^2}{n_2^2} + \frac{x_3^2}{n_3^2} = 1 \quad (27)$$

This surface is a convenient geometric representation for finding the optical eigenmodes of the displacement vector \vec{D} for a given direction of propagation. These eigenmodes are found by finding the principal axes of the ellipse normal to the propagation direction. Associated with each eigenmode is a corresponding index of refraction, equal to the ellipse radius along each principal axis.

2.3 Photoelastic coupling

The photoelastic effect is usually described in terms of an elastically induced perturbation of the impermeability tensor mediated by a fourth rank elastooptic tensor, which has nonzero components in all materials[2, 4].

$$\Delta\eta_{ij} = \Delta \left(\frac{1}{n^2} \right)_{ij} = \mathbf{p}_{ijkl} \mathbf{S}_{kl} \quad (28)$$

The symmetry of the index ellipsoid in i and j, and the strain tensor in k and l result in the symmetry relations for the strain-optic tensor $\mathbf{p}_{ijkl} = \mathbf{p}_{jikl} = \mathbf{p}_{ijlk} = \mathbf{p}_{jilk}$. Because the index perturbations due to the photoelastic effect are small we can use the relationship $dn = -\frac{1}{2}n^3 d \left(\frac{1}{n^2} \right)$ to write

$$(\Delta n)_{ij} = -\frac{n^3}{2} \mathbf{p}_{ijkl} \mathbf{S}_{kl} \quad (29)$$

Thus the perturbation of the optical index is proportional to the magnitude of the applied strain, and as long as the appropriate photoelastic tensor coefficient is nonzero there will be a resulting phase modulation of a properly polarized optical wave passing through the medium.

An acoustic eigenmode plane wave as in Eq. (1), will induce a strain wave of the form

$$\mathbf{S}(\vec{x}, t) = \frac{1}{2} W \hat{S}_{mn} \cos(\Omega t - \vec{K} \cdot \vec{x}) \quad (30)$$

Where \hat{S}_{mn} is a unit strain tensor for the given mode. This will induce a periodic travelling wave volume dielectric tensor perturbation that will couple the *i*th polarization component of the input mode with the *j*th polarization component of the output mode

$$\Delta\epsilon_{ij}(\vec{x}, t) = \frac{W}{2} \epsilon_{ik} (\mathbf{p}_{klmn} \hat{S}_{mn}) \epsilon_{lj} \cos(\Omega t - \vec{K} \cdot \vec{x}) \quad (31)$$

For an isotropic medium this corresponds to a perturbation of the index of refraction given by

$$\Delta n_{ij}(\vec{x}, t) = -\frac{n^3}{2} W \mathbf{p}_{ijmn} \hat{S}_{mn} \cos(\Omega t - \vec{K} \cdot \vec{x}) = \delta n_0 \cos(\Omega t - \vec{K} \cdot \vec{x}). \quad (32)$$

This index grating of amplitude $\delta n_0 = -\frac{n^3}{2} W \mathbf{p}_{ijmn} \hat{S}_{mn}$ can diffract an incident optical plane wave, of polarization *i* into a diffracted beam with polarization *j*, if the appropriate photoelastic tensor element is nonzero, and as long as both energy and momentum are conserved. This results in two conservation equations for the incident and diffracted optical waves.

$$\vec{k}_d = \vec{k}_i \pm m \vec{K}_a \quad m = 0, 1, 2, \dots N \quad (\text{momentum conservation}) \quad (33)$$

$$\omega_d = \omega_i \pm m \Omega_a \quad m = 0, 1, 2, \dots N \quad (\text{energy conservation}) \quad (34)$$

$$(35)$$

The plus and minus signs in these equations correspond to the annihilation or creation of *m* phonons, respectively.

With near normal incidence, many orders are simultaneously created and we are said to be in the Raman-Nath regime, which is illustrated in Figure 3a. When the width of the acoustic wave in the direction of light propagation greatly exceeds the characteristic length $L_0 = \frac{n\Lambda_0^2 \cos \theta}{\lambda}$, indicating that an optical beam encounters several acoustic wavefronts as it traverses the acoustic wave at an angle θ , then the interaction is in the Bragg regime. When the incident light is at

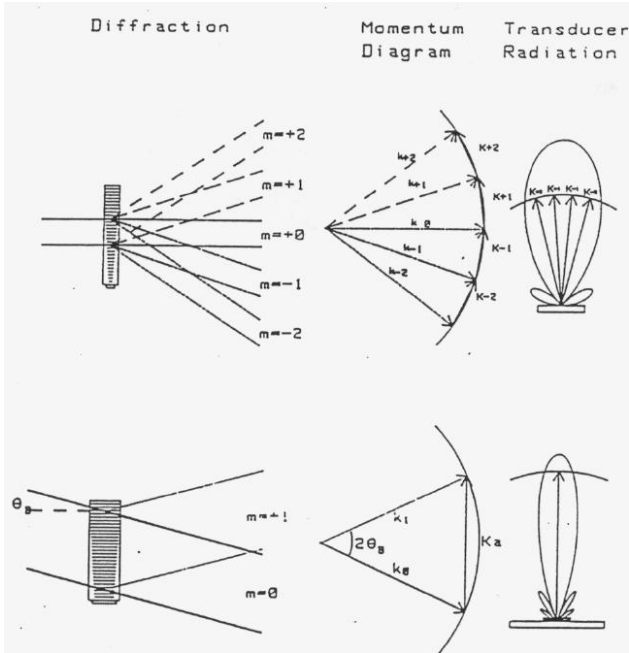


Figure 1: a) The Raman-Nath regime of acousto-optic diffraction, b) The Bragg regime, with incidence at the Bragg angle.

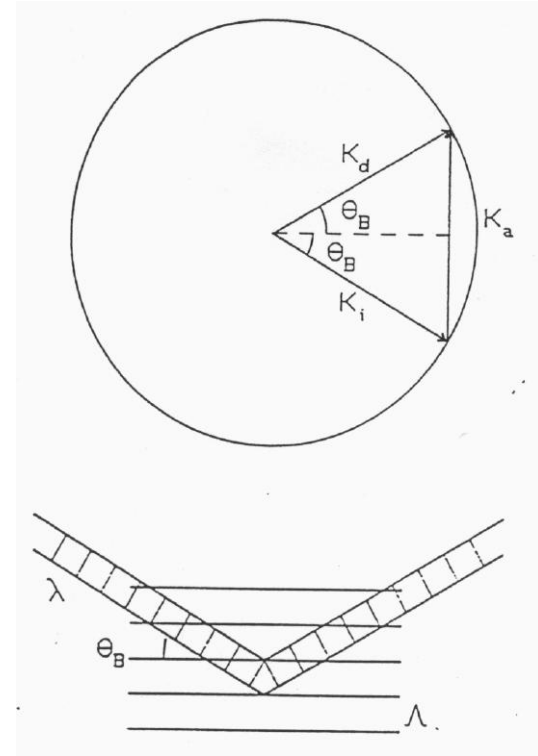


Figure 2: a) Momentum matching conditions for isotropic Bragg diffraction in the interaction plane, b) coherent reflection off of individual acoustic wavefronts.

the Bragg angle with respect to the acoustic wave, then only one diffracted order is allowed with either $m = \pm 1$, which is illustrated in Figure 3b. This describes a quantum mechanical particle scattering interaction between three particles, the incident photon, the diffracted photon, and the acoustic phonon. In order to conserve energy the diffracted photon is doppler shifted by the moving phase grating by an amount exactly equal to the frequency of the acoustic phonon. This frequency shift can only be observed interferometrically, and it plays a key role in the heterodyne detection experiment in the lab. The momentum matching equation (26) describes a closed triangle in momentum space whose vertices, corresponding to the incident and diffracted wave, must be allowed optical eigenmodes. This is illustrated in Figure 4a for the isotropic case, such as would be observed in fused silica, in which case the closed triangle is isosceles and $|\vec{k}_i| = |\vec{k}_d|$, because the change in the optical frequency and energy due to the acoustic wave is less than one part in 10^6 . The angles between the acoustic plane wavefronts and the incident and diffracted optical beams are the same, and are called the Bragg angle θ_B . This direction corresponds to constructive interference between different portions of the diffracted beam. It can be derived by modelling each acoustic wavefront as a partially reflecting mirror, and requiring the reflected portion from adjacent wavefronts to add up in phase as is illustrated in Figure 4b. The resulting Bragg angle is given by

$$\theta_B = \sin^{-1} \frac{|K|}{2|k|} = \sin^{-1} \frac{\lambda}{2n\Lambda} = \sin^{-1} \frac{\lambda f}{2v_a n} \approx \frac{\lambda f}{2v_a n} \quad (36)$$

The angular deviation of the diffracted light is seen to be proportional to the frequency of the applied acoustic wave in the small angle approximation, which is the basis of many acousto-optic

systems.

2.4 1-Dimensional coupled mode solutions

One method of solving the 1-dimensional acousto-optic coupled mode equation is to assume a perfectly phase matched interaction, while also assuming that the modal amplitudes are only a function of the z coordinate, even though this is not completely rigorous. For an incident optical plane wave with polarization \hat{E}_0 and incident amplitude $A_0(0)$, that is diffracted by the acoustic wave into a plane wave with polarization \hat{E}_1 whose amplitude grows with interaction distance z within the AO medium, the total field can be written in the interaction regime $0 < z < L$, as

$$\vec{E}(\vec{x}, t) = A_0(z)\hat{E}_0e^{-i(\omega_0t-k_{x0}x-k_{z0}z)} + A_1(z)\hat{E}_1e^{-i(\omega_1t-k_{x1}x-k_{z1}z)} \quad (37)$$

In the presence of the dielectric perturbation given by Eq. 24 the two modes are coupled, provided that momentum and energy are conserved. The total field is a solution of the inhomogenous wave equation

$$\nabla^2 \vec{E}(\vec{x}, t) - \mu(\epsilon + \delta\epsilon(\vec{x}, t)) \frac{\partial \vec{E}(\vec{x}, t)}{\partial t^2} = 0 \quad (38)$$

The individual fields with constant amplitudes are solutions of the unperturbed homogenous wave equation which allows us to substitute the total field and the acoustically induced dielectric perturbation in the wave equation, and obtain for the one dimensional interaction configuration

$$\begin{aligned} & \sum_{m=0,1} \hat{E}_m e^{-i(\omega_m t - k_{xm} x - k_{zm} z)} \left[\frac{\partial^2}{\partial z^2} - 2ik_{zm} \frac{\partial}{\partial z} \right] A_m(z) \\ & + \frac{W}{2} \epsilon_{ik} (\mathbf{p}_{klmn} \hat{S}_{mn}) \epsilon_{lj} \left[e^{-i(\Omega t - K_x x - K_z z)} + c.c. \right] \mu \sum_{l=0,1} \omega_l^2 A_l(z) \hat{E}_l e^{-i(\omega_l t - k_{xl} x - k_{zl} z)} = 0 \end{aligned} \quad (39)$$

$$(40)$$

The adiabatic condition allows us to assume that the modal amplitudes $A_m(z)$ are slowly changing in z compared to an optical wavelength so that we can neglect the second order spatial derivative. We now require that the coefficients of $\hat{E}_m e^{-i(\omega_m t - k_{xm} x - k_{zm} z)}$ vanish for $m = 0, 1$, in order to obtain a phase synchronous transfer of power between the modes. This requires that $k_{x1}x - k_{z1}z = k_{x0}x - k_{z0}z \pm K_x x - K_z z$ and $\omega_1 = \omega_0 \pm \Omega$, which are the familiar momentum and energy conservation conditions.

For Bragg interactions only a single order has a totally phase synchronous interaction with the input fields so we only get coupling to a single mode. This results in the well known coupled mode equations for perfectly phase matched interactions.

$$\frac{dA_0(z)}{dz} = -i\kappa A_1 \quad (41)$$

$$\frac{dA_1(z)}{dz} = -i\kappa^* A_0. \quad (42)$$

$$(43)$$

Where the coupling constant is found from the incident and diffracted polarization vectors left and right projected onto the dielectric perturbation tensor.

$$\kappa = \frac{\omega}{4} \hat{E}_0^* \cdot \Delta\epsilon \hat{E}_1 = \frac{\omega}{4} |E_{0i}^* \cdot \frac{W}{2} \epsilon_{ik} (\mathbf{p}_{klmn} \hat{S}_{mn}) \epsilon_{lj} E_{1j}| \quad (44)$$

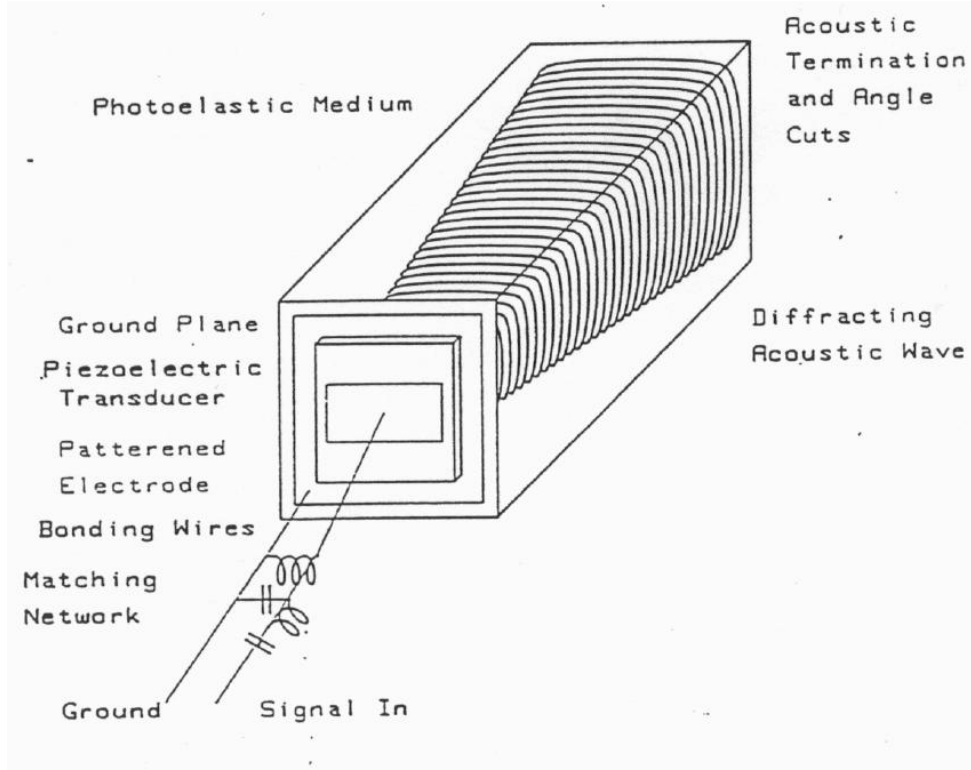


Figure 3: Schematic diagram of an acousto-optic device.

The solution of the coupled mode equation with the implied boundary condition of $A_1(0) = 0$, yields the perfectly coupled mode solution for $z > 0$

$$A_0(z) = A_0(0) \cos |\kappa|z, \quad (45)$$

$$A_1(z) = -i \frac{\kappa}{|\kappa|} A_0(0) \sin |\kappa|z. \quad (46)$$

$$(47)$$

So the optical field is seen to oscillate back and forth between the incident and diffracted field each distance $2L_m = \pi/|\kappa|$, as the beams propagate in the z direction. Complete power transfer occurs from the input to the diffracted mode after a distance of z propagation given by L_m . The diffraction efficiency is the ratio of the incident optical intensity to the intensity transferred to the diffracted beam in a distance L , and it is given by

$$\frac{I_2}{I_1} = \frac{|A_1(L)|^2}{|A_0(0)|^2} = \sin^2 |\kappa|L \quad (48)$$

Thus given the amplitude W of the acoustic mode \hat{S}_{kl} , the interaction length L , the input polarization \hat{E}_0 , the output polarization \hat{E}_1 , and the material tensors ϵ_{ij} and \mathbf{p}_{ijkl} , we can find the percentage of light diffracted into the output beam.

2.5 Acousto-optic devices

An acousto-optic device is constructed by bonding an acousto-electric transducer onto a photoelastic medium, so that acoustic waves can be launched into the medium, and is illustrated in Figure 3.

The transducer is usually a piezoelectric crystal of thickness t_0 , metalized on both faces so that an electric field can be applied transversely in the k direction. This induces a strain through the third rank piezoelectric tensor \mathbf{d} , which can only exist in non-centrosymmetric materials.

$$\mathbf{S}_{ij}(t) = \mathbf{d}_{ijk}E_k = \mathbf{d}_{ijk}v_k(t)/t_0 \quad (49)$$

The appropriate choice of transducer crystal cut and orientation are used to produce the desired polarization of the acoustic wave which is launched into the photoelastic medium. The time dependent strain within the transducer is coupled into the photoelastic medium with a frequency dependent efficiency dictated by the acoustic impedance matching of the transducer and bonding layers. The frequency dependence of the electro-acoustic conversion $R(f)$, is due to the electrical matching network, the transducers resonant bandwidth and the mechanical coupling efficiency bandshape. By applying a sinusoidally varying electric field to the transducer, that is within its acoustic resonant bandwidth, we can launch a propagating acoustic wave into the photoelastic medium. Since the transducer has a finite spatial aperture the harmonic acoustic field will have a spatial angular divergence. The angular spectrum of the transducer is given by the Fourier transform of its aperture $p(y, z)$, scaled by the appropriate acoustic wavelength. The angular divergence of the transducer in the interaction dimension coupled with the phase matching condition is what determines the acousto-optic bandshape of the device. For an isotropic device with a simple uniform rectangular transducer of length L and height H the transducer radiation pattern acoustic angular spectrum in the interaction dimension is given by the simple 1-D transform $\text{sinc}^2(L\beta_z/\Lambda)$. The resulting isotropic acousto-optic bandshape can be derived from the viewpoint of phase mismatched interaction, or from the viewpoint of selecting the appropriate angular component from the transducer radiation field in order to obtain perfect phase matching, and these different interpretations are schematically illustrated in Figure 4a. The isotropic acousto-optic bandshape is given in terms of the perfectly matched on axis frequency f_m , normalized by the center frequency f_0 , and the normalized interaction length, as a function of the normalized frequency $F = f/f_0$.

$$W(F) = \text{sinc} \left[\frac{L}{2L_0} F(F_m - F) \right] \quad (50)$$

Thus the transducer length L determines the acousto-optic bandwidth, and it determines the effective interaction length as well, thereby affecting the diffraction efficiency.

In the tangentially degenerate approach to birefringent phase matching[5], the acoustic wave vector is tangent to the locus of fast diffracted wave vectors at the symmetric center frequency f_1 , and the peak of the transducer angular spectrum intersects the diffracted wave vector surface at two frequencies $f_m^\pm = f_0 \pm \Delta f/2$. The resulting birefringent acousto-optic bandshape is broadened, and is given in terms of normalized frequency variables.

$$W(F) = \text{sinc} \left[\frac{L}{2L_0} (F - F_1)^2 - \frac{\Delta F}{2} \right] \quad (51)$$

When the symmetrical frequency is at midband and phase matched $\Delta f = 0$, then $f_m = f_0 = f_1$, and the tangentially matched acousto-optic bandshape has a simple quadratic frequency dependent phase mismatch term $(F - 1)^2$. The decreased transducer angular bandwidth needed by a device operating in the tangentially degenerate phase matching regime is illustrated in Figure 9b. The transducer can be longer and a larger interaction length results in a greater diffraction efficiency, and the bandshape becomes symmetrical.

The transducer height H determines the degree of collimation in the orthogonal dimension which determines the diffraction limited usable aperture time. For the isotropic acoustic case the

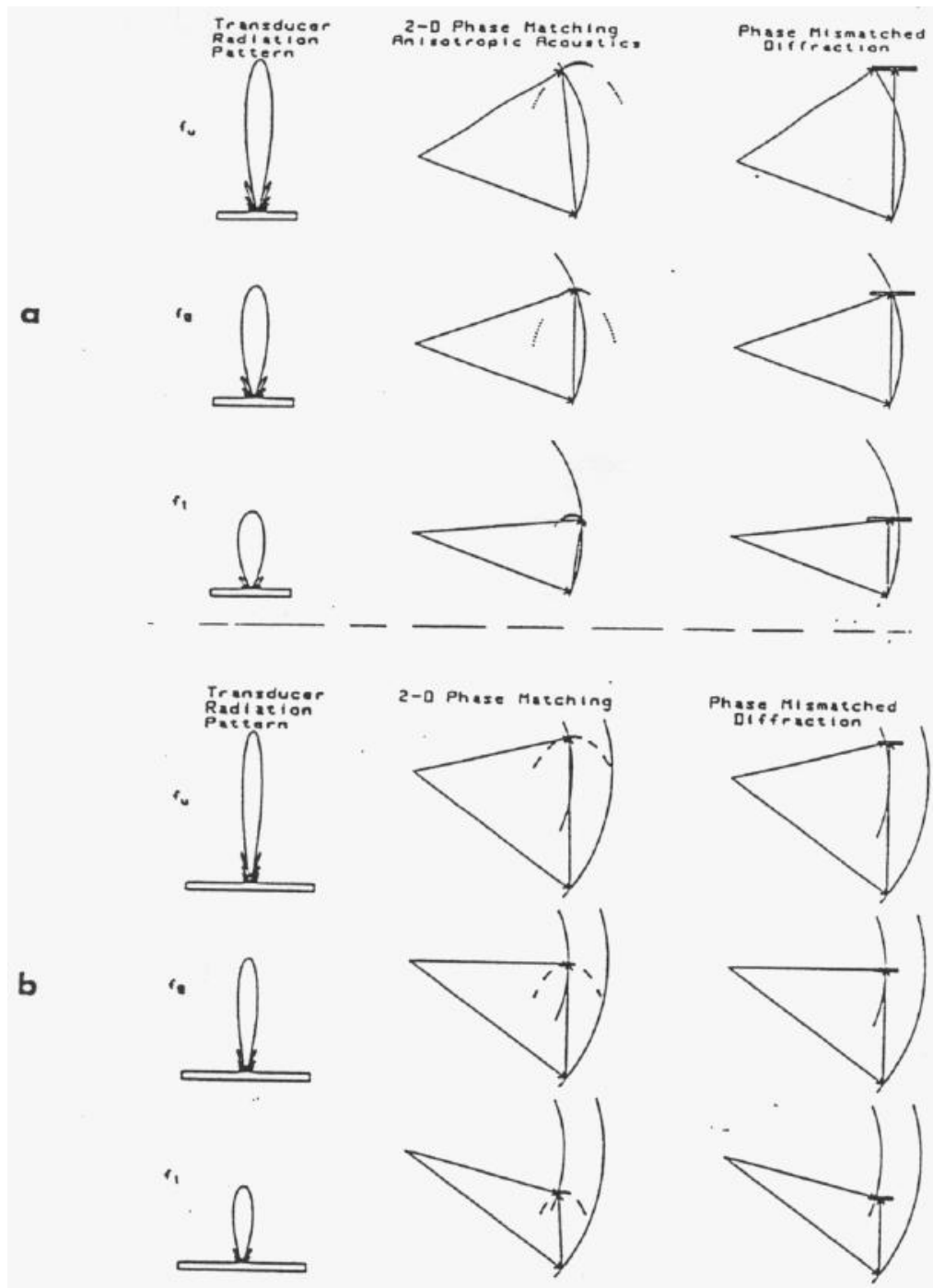


Figure 4: Transducer angular radiation pattern, 2-dimensional phase matching, and phase mismatched diffraction, for the lower, midband and upper frequencies of a) an isotropic device and b) a tangentially degenerate phase matched device.

transducer radiation pattern remains within the near field in the height dimension for a distance $D = H^2/\Lambda$, which is equal to the distance that the transducer angular spectrum at the 4dB half width intersects the transducer geometric shadow. In the anisotropic acoustic case the near field in the height dimension is modified by the acoustic curvature factor giving a near field distance $D' = H^2/\Lambda(\frac{1}{2} - b_y)$. The transducer area LH relates to the acoustic power density through the equation $P_a = \frac{1}{2}\rho_m v_a^2 |S|^2 LH$. and thus determines the optical diffraction efficiency in terms of the electrical power input to the transducer. A tradeoff between the diffraction efficiency and the interaction bandwidth can be tailored by an appropriate choice of the transducer length to height ratio L/H .

A Bragg cell or acousto-optic deflector (AOD) is the basic electrical to optical transducer used in this lab. From the system point of view this device is modelled as a 1-D travelling wave modulator with a finite aperture window. Thus when a temporal signal $s(t)$ is applied to the device, the resulting transmission function of an idealized device is represented as

$$t(x, y) = \alpha s(t - x/v_a)w(x) \quad (52)$$

The acoustic velocity v_a is taken to be the nominal velocity along the symmetry axis normal to the transducer. The window function $w(x)$ is the product of the device finite aperture window with the acoustic attenuation, and the input optical beam gaussian profile is often included as well, thereby making the window function a hybrid window of the induced polarization field which is the product of input field and dielectric perturbation.

2.5.1 Acoustic Phased-Arrays for increased Efficiency-Bandwidth Product

Another technique used to increase the efficiency-bandwidth product of a deflector is to use a beamsteering acoustic phased-array-transducer. These transducers produce a narrow angular radiation lobe, ideal for high diffraction efficiency, but generally poor for bandwidth, and then they steer this acoustic radiation lobe as the frequency is varied in the direction necessary to phase match over a wide bandwidth. Two types of phased arrays are commonly used, the constant phase delay phased arrays, and the constant time delay phased arrays, and these are illustrated in Figure 5. A constant phase delay of 180 degrees between adjacent transducer array elements can be accomplished by applying the RF to alternate transducers which lie on top of a voltage dividing floating ground plane. Such an array produces two main acoustic lobes which both steer towards the normal as the frequency is increased. Only one of these lobes is utilized in a typical beam steering acoustooptic device, and the power in the other lobe is wasted. When 3 RF phases 120 degrees apart are used to drive 3 alternating transducer phases, then only one main acoustic beam is produced, thereby doubling the efficiency of such a device, however the complexity of 120 degree hybrids detracts from the attractiveness of this scheme. An alternate approach to producing a single acoustic beam which steers with frequency is the constant time delay phased array implemented as a stepped staircase transducer, where the step size is half the midband acoustic wavelength $\Lambda_c/2$ as illustrated in Figure 5b. In both of these beam steering techniques the locus of acoustic momentum vectors trace out a straight line orthogonal to the transducer, but offset by the fundamental grating frequency of the transducer, so that the resulting acoustic momentum vector is given by $\vec{K}_a = 2\pi v_a/f\hat{z} + \pi/d\hat{x}$, where f is the applied frequency, d is the width of each phased array element, and \hat{x} is in the direction of the transducer elements. As the Bragg cell is rotated this locus of acoustic beams is brought into tangency with the optical momentum surface, in an analogous manner as in anisotropic diffraction, thereby maintaining a small phase mismatch over a wide bandwidth because of the quadratic deviation from perfect phase matching. However,

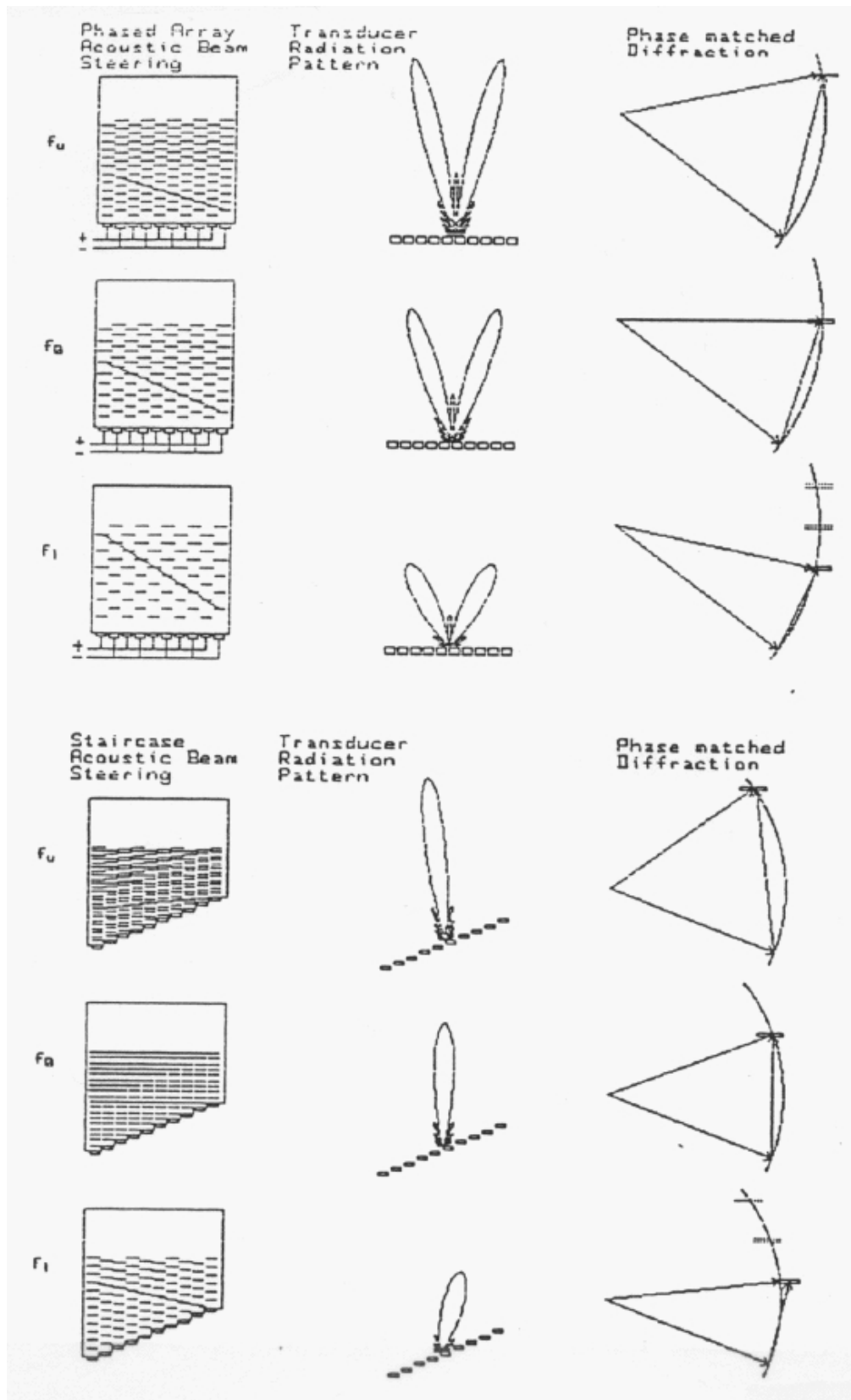


Figure 5: Phased array acoustic beam steering techniques showing acoustics, transducer angular radiation patterns and Bragg matched diffraction. a) alternating phase beam-steering-array, b) beam steering array with a stepped staircase transducer.

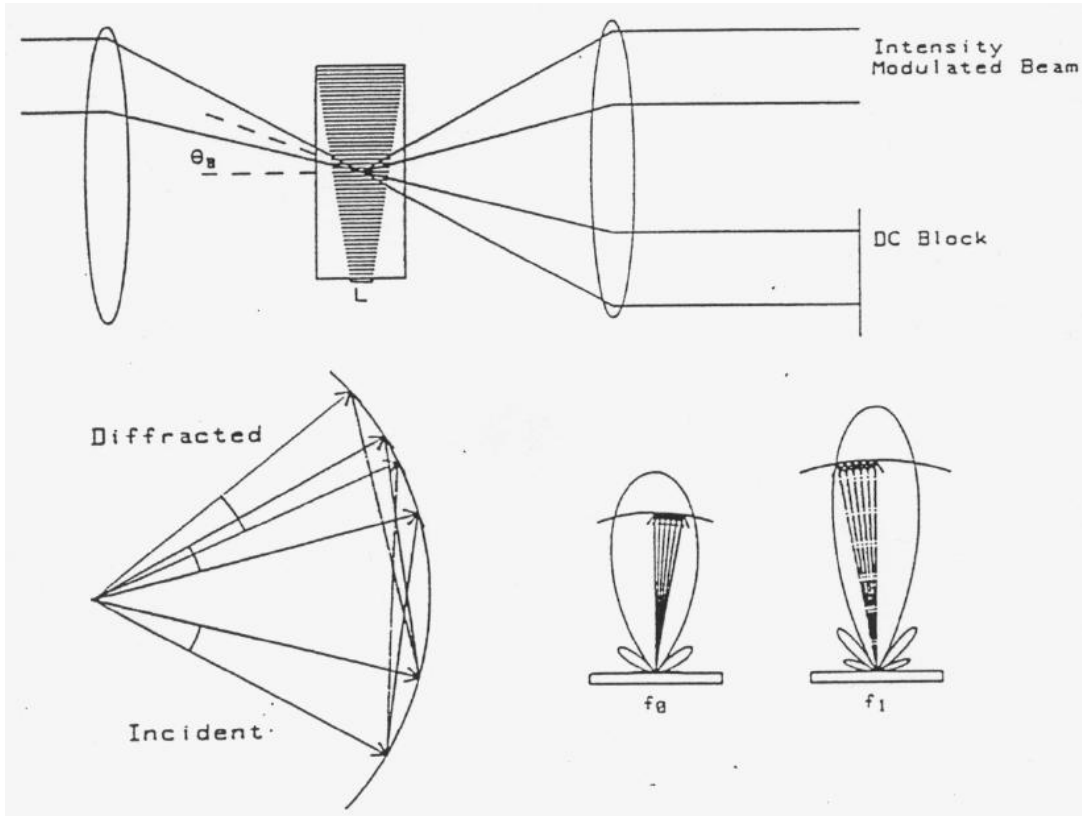


Figure 6: An acousto-optic modulator operating in the Bragg regime.

when such a beam steering array is rotated to the other Bragg angle, then the locus of acoustic momentum vectors cuts through the optical momentum surface with a linear dependence of the momentum mismatch on frequency, seriously degrading the bandwidth for that order.

2.6 Acousto-optic modulators

Another important device is the acousto-optic point modulator or AOM, which is similarly constructed by bonding an acousto-electric transducer to a photo-elastic medium. The principal difference between an AOM and an AOD is that the AOM is used with a tightly focussed optical spot incident on the center of the acoustic column and the AOD is illuminated with a collimated wave. This is because the modulator must have a quick access time in order to achieve wide modulation bandwidth, which is the inverse of the acoustic propagation time across the beam waist of the focussed spot[6]. In order to be able to modulate each spatial frequency component of the focussed optical field there must be a corresponding phase matched frequency component of the diffracting acoustic wavefront, thereby dictating a short transducer length L . This leads to a tradeoff between diffraction efficiency and access time. The Bragg angle centered focussing incident beam and the diverging diffracted wave must be separated in the Fourier plane for single sideband suppressed carrier modulation, where the diffracted intensity is proportional to the envelope modulation of the acoustic carrier. This leads to a requirement that the carrier frequency be several times higher than the access time limited modulation bandwidth, which in turn requires that several acoustic phase fronts be contained within the optical beam waist. The intensity modulation of the diffracted beam by the envelope of the acoustic signal can be considered to be a mixing of the carrier with the sidebands which are responsible for the amplitude modulation.

When the modulation frequency increases the diffraction angle of the sidebands increases so that less of the diffracted cones from the sidebands overlap with the carrier. Optical heterodyning is optimized when the interfering components are colinearly propagating, so as the modulation frequency increases the modulation depth decreases, which is an alternative derivation of the modulator bandwidth limitation. This type of modulator arrangement is illustrated in Figure 6 , and the overlap of the diffracted waves in momentum space is illustrated for a frequency near the modulator 3dB bandwidth limitation.

A Bragg cell can be used as a modulator as well as a deflector, but because of the long transducers that are utilized with narrow acoustic angular spectrums a limit is placed on the amount of focussing of the incident optical wave that is allowed in order to have a phase matched acoustic component for each momentum component of the input optical field. This places a limit on how small of an aperture that can be illuminated and therefore limits the modulation bandwidth, or inverse access time. In order to use an AOD as a phase modulator the incident light should be collimated and incident at the Bragg angle. When pulsed laser illumination is used, access time is not a constraint, and the Bragg cell can be loaded with a phase shifted sinusoidal tone on each pulse. The diffracted phase modulated and doppler shifted plane wave is easily separated from the undiffracted wave in the Fourier plane since the AOD is deep within the Bragg regime and illuminated with a plane wave.

3 Appendix: Acousto-optic momentum matching

There are numerous derivations of the diffraction of light through a periodic dielectric perturbation such as an acousto-optic device or a volume hologram. In this appendix we present a Fourier description of this interaction that is the basis for the graphical design techniques used throughout this chapter. This Fourier description does not readily describe the diffraction from the dielectric perturbation in the large diffraction efficiency regime, however it does facilitate the design, evaluation, and synthesis of complex interaction geometries, such as that required in the acousto-optic photonic switch.

The equations describing volume holographic diffraction are simplified in the small diffraction efficiency limit (Born approximation). The following derivation provides an easy to visualize formulation that we believe is easier to use, particularly for those well versed in Fourier optics.[7, 8] It will be shown that the angular spectrum of the diffracted optical wave due to a monochromatic component of the signal applied to the transducer is given by the 3-D Fourier transform of the incident optical field and the monochromatic dielectric perturbation component, evaluated on the eigensurface in momentum space for the allowed propagating optical modes. The dielectric perturbation caused by the acoustic strain field is composed of monochromatic components, each of which produces a dielectric perturbation that is determined by the Fourier transform of the transducer aperture, painted onto the frequency scaled velocity surface, and convolved with the transform of the aperture function. This provides a complete description of the multitone, arbitrary geometry, arbitrary transducer structure, acousto-optic diffraction problem in the low efficiency regime.

We start with the wave equation for two coupled optical waves in a medium with a dielectric perturbation $\delta\epsilon(\vec{r}, t)$, given by

$$\nabla^2[E_i(\vec{r}, t) + E_d(\vec{r}, t)] + \frac{1}{c^2} \frac{\partial^2}{\partial t^2}[\epsilon_r + \delta\epsilon(\vec{r}, t)][E_i(\vec{r}, t) + E_d(\vec{r}, t)] = 0 \quad (53)$$

Where E_i and E_d are the incident and diffracted waves, ϵ_r is the materials relative dielectric tensor, and c is the speed of light. We seek a solution for the two waves in which each independently satisfies the wave equation when the dielectric perturbation vanishes. We separate equation 53 into the coupled equations for the incident field of frequency ω and each monochromatic angular frequency component, ω_m , of the diffracted field by including the harmonic temporal dependence and then using the orthogonality of different frequency components to enforce the conservation of energy.

$$\nabla^2 E_i(\vec{r}, \omega) + \frac{\omega^2 \epsilon_r}{c^2} E_i(\vec{r}, \omega) = -\frac{\omega^2}{c^2} = \sum_m \delta\epsilon^*(\vec{r}, \Omega_m) E_d(\vec{r}, \omega_m) \quad (54)$$

$$\nabla^2 E_d(\vec{r}, \omega_m) + \frac{\omega_m^2 \epsilon_r}{c^2} E_d(\vec{r}, \omega_m) = -\frac{\omega_m^2}{c^2} \delta\epsilon(\vec{r}, \Omega_m) E_i(\vec{r}, \omega) \quad (55)$$

The conservation of energy gives $\omega_m = \omega + \Omega_m$, and $\delta\epsilon(\vec{r}, \Omega_m)$ is the component of the time varying dielectric perturbation oscillating at angular frequency Ω_m . This can be further simplified by realizing that $\omega \approx \omega_m$ since $\Omega_m \ll \omega$. Additional simplifications result by assuming that the solutions for various different frequency components of the diffracted field $E_d(\vec{r}, \omega_m)$ will obey linear superposition of the solutions obtained in the presence of only a single frequency component of the dielectric perturbation, which is clearly valid in the Born limit. In the Born approximation, the incident wave E_i is much stronger than the diffracted wave E_d . With the right hand side of equation 54 approximately zero, the solution for the strong incident wave E_i is the naturally propagating eigenwaves in the media, which remain undepleted in the low diffraction efficiency regime.

We represent a particular frequency component of the diffracted wave as a transverse Fourier expansion of its plane wave components in the unperturbed media, which evolves along the nominal direction of propagation z .

$$E_d(\vec{r}, \omega_m) = \int \mathcal{E}_d^{\omega_m}(\vec{k}_t, z) e^{i\vec{k}_t \cdot \vec{r}} e^{ik_{zd}(\vec{k}_t)z} d\vec{k}_t \quad (56)$$

Where $k_{zd}(\vec{k}_t) = \sqrt{k_d^2 - \vec{k}_t \cdot \vec{k}_t}$ is the longitudinal component of the wavevector, $\vec{k}_t = \hat{x}k_{tx} + \hat{y}k_{ty}$ is the transverse component of the wavevector, and $k_d = 2\pi n_d(\vec{k}_t, \omega_m)\omega_m/c$ is the magnitude of the diffracted wavevector, where $n_d(\vec{k}_t, \omega_m)$ accounts for material anisotropy and dispersion (which is negligible over a frequency range Ω_m) and is simply equal to the index n in isotropic materials. Performing the derivative and subtracting the wave equation in the unperturbed media, equation 55 becomes

$$\int \left[2ik_{zd}(\vec{k}_t) \frac{\partial}{\partial z} \mathcal{E}_d^{\omega_m}(\vec{k}_t, z) + \frac{\partial^2}{\partial z^2} \mathcal{E}_d^{\omega_m}(\vec{k}_t, z) \right] e^{i\vec{k}_t \cdot \vec{r}} e^{ik_{zd}(\vec{k}_t)z} d\vec{k}_t = -\frac{\omega_m^2}{c^2} \delta\epsilon(\vec{r}, \Omega_m) E_i(\vec{r}, \omega) \quad (57)$$

In the slowly varying envelope approximation we can neglect the second derivative, $k_{zd}(\vec{k}_t) \frac{\partial}{\partial z} \mathcal{E}_d^{\omega_m}(\vec{k}_t, z) \gg \frac{\partial^2}{\partial z^2} \mathcal{E}_d^{\omega_m}(\vec{k}_t, z)$, giving

$$\int \int 2ik_{zd}(\vec{k}_t) e^{ik_{zd}(\vec{k}_t)z} \frac{\partial}{\partial z} \mathcal{E}_d^{\omega_m}(\vec{k}_t, z) e^{i(xk_{tx} + yk_{ty})} dk_{tx} dk_{ty} = -\frac{\omega_m^2}{c^2} \delta\epsilon(\vec{r}, \Omega_m) E_i(\vec{r}, \omega) \quad (58)$$

By taking the transverse Fourier transform in x and y , the equation for the evolution with z of the transverse spatial frequency components of the diffracted field E_d becomes

$$e^{ik_{zd}(k_x, k_y)z} \frac{\partial}{\partial z} \mathcal{E}_d^{\omega_m}(k_x, k_y, z) = \frac{i\omega_m^2}{2c^2 k_{zd}(k_x, k_y)} \int \int \delta\epsilon(\vec{r}, \Omega_m) E_i(\vec{r}, \omega) e^{-i(xk_{tx} + yk_{ty})} dx dy \quad (59)$$

This equation may be integrated directly to yield the field of the diffracted wave E_d at the exit face, $z = L$ of the media containing the dielectric perturbation.

$$\mathcal{E}_d^{\omega_m}(k_x, k_y, L) = \frac{i\omega_m^2}{2c^2 k_{zd}(k_x, k_y)} \int_{z=0}^{z=L} \mathcal{FT}_{xy} \{ \delta\epsilon(\vec{r}, \Omega_m) E_i(\vec{r}, \omega) \} e^{-ik_{zd}(k_x, k_y)z} dz \quad (60)$$

This last integral may be reformulated as an infinite integral by noting that the dielectric perturbation vanishes outside the region $z \in \{0, L\}$, where L is the crystal length. Extending the range of the z integration to infinity, we can substitute a three-dimensional Fourier transform

$$\mathcal{E}_d^{\omega_m}(k_x, k_y, L) = \frac{i\omega_m^2}{2c^2 k_{zd}(k_x, k_y)} \int \delta(k_z - k_{zd}(k_x, k_y)) \mathcal{FT}_{xyz} \{ \delta\epsilon(\vec{r}, \Omega_m) E_i(\vec{r}, \omega_m) \} dk_z \quad (61)$$

This is our key result. It states that the angular spectrum components of the diffracted field at the output of the media containing the weak dielectric perturbations is given by the 3-D Fourier transform of the product of the incident field and the dielectric perturbation, evaluated on the surface of the allowed propagating modes for the diffracted field.

In this formulation both momentum and energy are conserved exactly, which is in contrast to most other treatments which consider momentum mismatch to be a violation of momentum conservation rather than a decrease of the Fourier amplitude of a finite dielectric perturbation as shown above. It should be noted that $k_{zd}(\vec{k}_t)$ is linearly dependent on the frequency of the diffracted beam (neglecting dispersion), so that the sampling ellipsoidal momentum surface represented by the δ function grows proportional to the diffracted beams frequency. However, this effect is very small for acousto-optics, $\Omega_m/\omega < 10^{-6}$, and can often be safely treated as a single sampling surface cutting through the uncertainty distribution of the product of the incident wave and the dielectric perturbation.

Some of the key concepts of this derivation are presented in Figure 7. The acousto-optically induced polarization responsible for radiating the diffracted field is, in the Born limit, given by the product of the incident optical field and the perturbing acoustic field. For an infinite medium illuminated by a single incident plane wave and containing a single infinite acoustic plane wave perturbation the resulting acousto-optically generated polarization is given by

$$\vec{P}^{AO}(\vec{r}, t) = \epsilon_0 \bar{\epsilon}_r \bar{\bar{\bar{p}}} \bar{\bar{A}} e^{i\vec{K}\cdot\vec{r}} e^{-i\Omega t} \vec{E}_i e^{i\vec{k}\cdot\vec{r}} e^{-i\omega t} \bar{\epsilon}_r \propto e^{i(\vec{k}+\vec{K})\cdot\vec{r}} e^{-i(\omega+\Omega)t} \quad (62)$$

where $\bar{\epsilon}_r$ is the relative dielectric tensor, $\bar{\bar{\bar{p}}}$ is the 4th rank photoelastic tensor, \vec{E}_i is the incident optical field polarization, and $\bar{\bar{A}}$ is the acoustic strain tensor. This equation shows that the wavevector of the acousto-optically generated polarization field is given by the sums of the wavevectors of the incident and perturbation fields, and the frequency of this travelling polarization field is given by the sums of their respective frequencies. Graphically this can be represented as a momentum of the polarization field which is given by the vector sum of the momentums of the incident and acoustic fields. Multiple simultaneous acoustic waves with different K-vectors will each produce a polarization field with the corresponding vector sum of the momentums of the contributing fields as shown in the figure as two vector sum triangles.

For finite materials and finite aperture incident beams and acoustic perturbation fields, the problem can be decomposed into individual Fourier components. This is accomplished with the 3-D Fourier transform of the product of the unperturbed incident field and the dielectric perturbation used in equation 61. This is illustrated in 2-D in the middle of figure 7 for the case of a rectangular profile incident beam of width A interacting with a rectangular boundary acoustic perturbation of

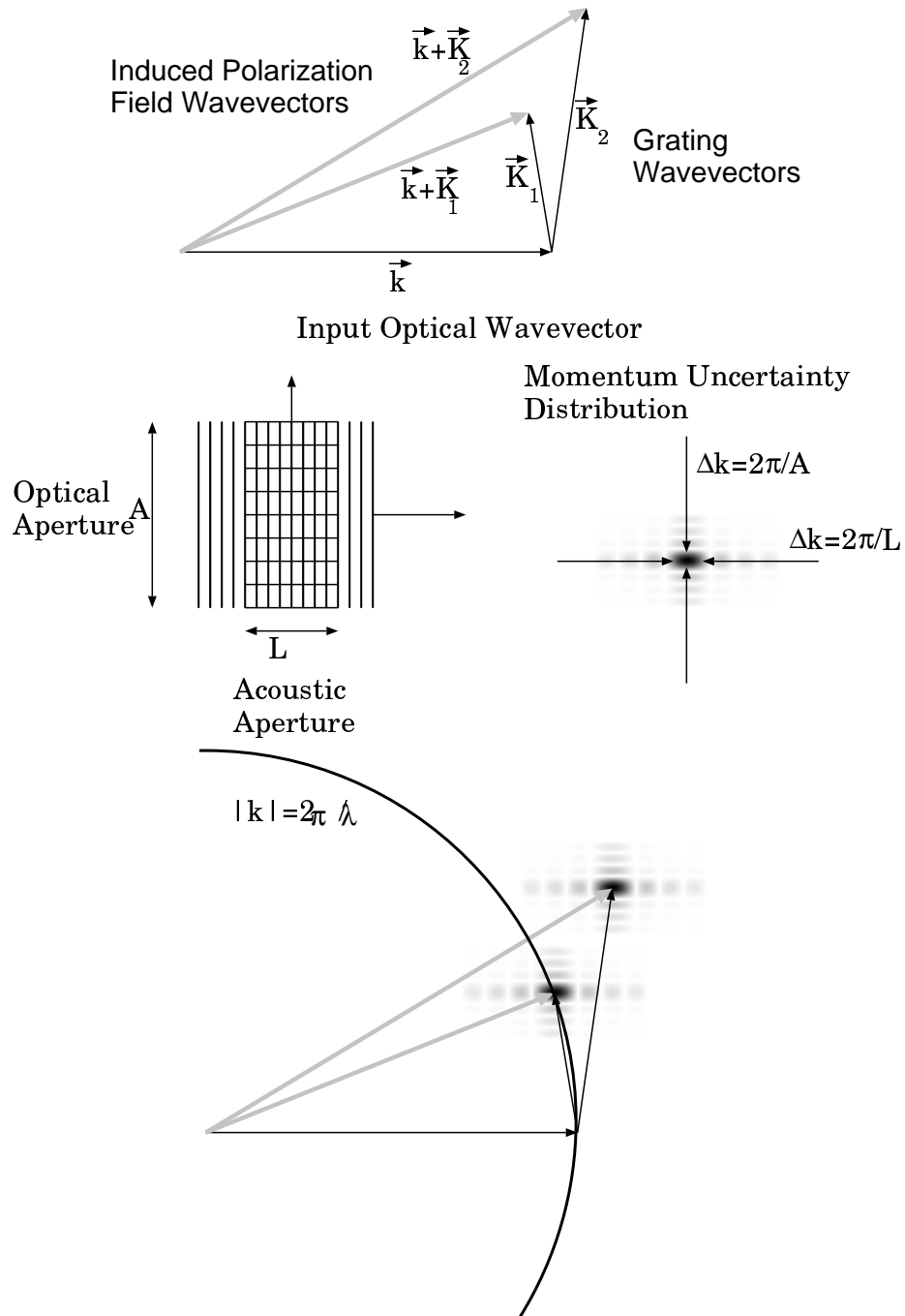


Figure 7: Graphical representation of the steps in the derivation of the diffracted field using a pictorial representation of momentum space.

width L . The Fourier transform of the product of these two rectangular boundaries produce a 2-dimensional (possibly skewed) sinc distribution of Fourier uncertainty, representing the amplitude and phase of all of the individual infinite plane wave Fourier components that must be combined to produce the spatially finite polarization field. In this case this sinc distribution has a half power width (actually $\approx 4\text{dB}$ width) given by $\Delta k_z = 2\pi/L$ and a height given by $\Delta k_x = 2\pi/A$. Although there are numerous sidelobes extending to infinity in Fourier space, most of the power in the acoustooptically generated polarization wave is contained within the $\frac{2\pi}{L} \times \frac{2\pi}{A}$ “*uncertainty box*” which is a useful abstraction and shorthand representation of the full Fourier distribution of uncertainty used throughout this chapter.

At a particular incidence angle, illustrated in the bottom of the figure, the relative amplitude and angular distribution of the diffracted optical field is given by the intersection of the momentum surface of freely propagating optical waves with the distribution of Fourier uncertainty of the acoustooptically generated polarization wave. The optical momentum surface is derived from the solution of Fresnel’s equation for the ordinary and extraordinary waves $n_o(\theta, \phi)$ and $n_e(\theta, \phi)$ times $2\pi/\lambda$. The optical momentum surface slices through the distribution of Fourier uncertainty of the polarization wave, selecting only the components that are exactly phase matched with the freely propagating optical waves to be produced as radiated waves. These components exactly satisfy the conservation of momentum, just as the Doppler shift of the diffracted field exactly satisfies the conservation of energy. The resulting angular distribution of the amplitude of the diffracted optical field (eg the sinc function) painted across the surface of allowed propagating optical eigenmodes, indicates the finite angular resolution of the diffracted field that is due to the fact that it emerges from a finite aperture medium, and inevitably diffracts with an angular half width of at least $\Delta\theta = \lambda/A$. The absolute amplitude of the diffracted waves requires in addition knowledge of p_{eff} , which is determined by the photoelastic and dielectric material tensors (including the piezoelectric-electrooptic contribution), the eigenpolarizations of the incident and diffracted optical waves, and the strain tensor of the acoustic wave.

3.1 Acoustic diffraction

For the acoustooptic case utilizing a planar transducer radiating into an infinite half space, specifically for a transducer with variations due to phased array patterning only along the z' -direction, we can write a simplified expression for the dielectric perturbation in the $x' - z'$ Bragg interaction plane. (The z' direction is often nearly along the previous z for typical small angle Bragg diffraction geometries, but is not necessarily so. However for convenience we will drop the prime in the subsequent analysis) Given a velocity surface for a pure mode in the Bragg plane as a solution to the acoustic Christoffel equation given by $v_a(\theta)$, [1] and a one-dimensional transducer structure defined by the aperture profile $p(z)$, then applying a monochromatic excitation at frequency Ω_m to the transducer will produce a dielectric perturbation proportional to [9]

$$\delta\epsilon(\vec{r}, \Omega_m) \propto e^{i\Omega_m t} \int p_{eff} P(k_z) e^{ik_z z} e^{-ik_x(k_z, \Omega_m)x} dk_z \quad (63)$$

where p_{eff} is the effective photoelastic constant which depends on interaction geometry, polarization and material coefficients, $P(k_z) = \int p(z) e^{-ik_z z} dz$ is the Fourier transform of the transducer profile, and

$$k_x(k_z, \Omega_m) = \frac{\Omega_m}{v_a} \tan^{-1} \left(\frac{k_z}{k_x(k_z, \Omega_m)} \right) \quad (64)$$

is the self-consistent longitudinal momentum component for an acoustic wave of frequency Ω_m propagating at an angle $\theta = \tan^{-1}[k_z/k_x(k_z, \Omega_m)]$. Now for an arbitrary superposition of frequencies applied to the transducer, the overall dielectric perturbation is simply the linear combination

$$\delta\epsilon(\vec{r}, t) \propto \int S(\Omega_m) e^{i\Omega_m t} \int p_{eff} P(k_z) e^{ik_z z} e^{-ik_x(k_z, \Omega_m)x} dk_z d\Omega_m \quad (65)$$

where $S(\Omega_m) = \int s(t) e^{-i\Omega_m t} dt$ is the Fourier transform of the applied signal $s(t)$. Finally, we must add the effects of finite aperture and acoustic attenuation. The anisotropic character of the acoustic absorption can be included by including the imaginary part of $k_x(k_z, \Omega_m)$, which corresponds to the frequency dependent (typically following the f^2 law) surface of acoustic absorption, just as the real part corresponds to the acoustic momentum surface. The effect of the finite length, L , of the transducer or photoelastic medium in the direction of optical propagation is imbedded in the 3-D Fourier transform in equation 61. The effect of the finite aperture of the device in the direction of acoustic propagation is also contained in the 3D Fourier transform, but can instead be incorporated here as a convolution of the distribution of acoustics in momentum space with the transform of the aperture function.

$$\delta\epsilon_A(k_x, k_z, t) \propto \int \int a(z) \delta\epsilon(\vec{r}, t) e^{i2\pi(xk_x + zk_z)} dx dz = A(k_z) * \mathcal{FT}_{xyz} \{ \delta\epsilon(\vec{r}, t) \} \quad (66)$$

where $A(k_x) = \mathcal{FT}_x \{ a(x) \}$. Typically the hybrid aperture function $a(x)$ is given by the product of the rectangular aperture, acoustic attenuation, and the incident optical Gaussian beam profile, (however when the Gaussian profile is already incorporated in the incident field then it should not be included here as well) $a(z) = \text{rect} \left[\frac{z}{A} \right] e^{-\alpha(z-A/2)f^2}$. For large angle acoustic beamsteering the acoustic attenuation is direction dependent, so should be incorporated in the angular spectrum of the transducer as the imaginary part of k_x instead. This gives a complete prescription for the time varying dielectric perturbation produced by an acoustooptic device in both real and momentum space, which can be combined with equation 61 to calculate the full optical diffracted field in the low diffraction efficiency regime for arbitrary incident beam profiles, transducer structures, and acoustooptic geometries.

An example of the frequency dependent acoustic momentum space distribution of a phased array transducer is schematically illustrated in Figure 8. On the left is shown the alternating phase transducer structure in real space, with a center to center transducer spacing of d and period $2d$, and the launched acoustic waves in the near field. The tilted composite wavefronts produce plus and minus beam steering orders K_{a+} and K_{a-} as well as other higher order lobes. The phase profile at the medium boundary is shown underneath the transducer, along with the principal Fourier components of its spatial harmonic decomposition. It is common in acoustooptics to consider the angular radiation pattern of the transducer, which consists of the element function and the grating lobes. As the frequency varies the scale factor of the transducer and its angular diffraction function changes and the beams steer. The anisotropies of the acoustics are accounted for by painting the angular radiation function of the transducer array onto the frequency scaled momentum surface self consistently. In the momentum space approach, the 1-dimensional Fourier transform of the transducer produces a set of boundary conditions for the radiating acoustics which are satisfied by projecting this distribution of transverse momentum onto the appropriate frequency scaled acoustic momentum surface, and then convolved with the transform of the device aperture in the acoustic propagation direction. For arbitrary acoustic anisotropy, (and even in the presence of dispersion such as with Love waves), the conserved quantity is the transverse momenta of the transducer array, represented by $K_{bs} = \pi/d$. As the frequency varies, the locus of the maxima

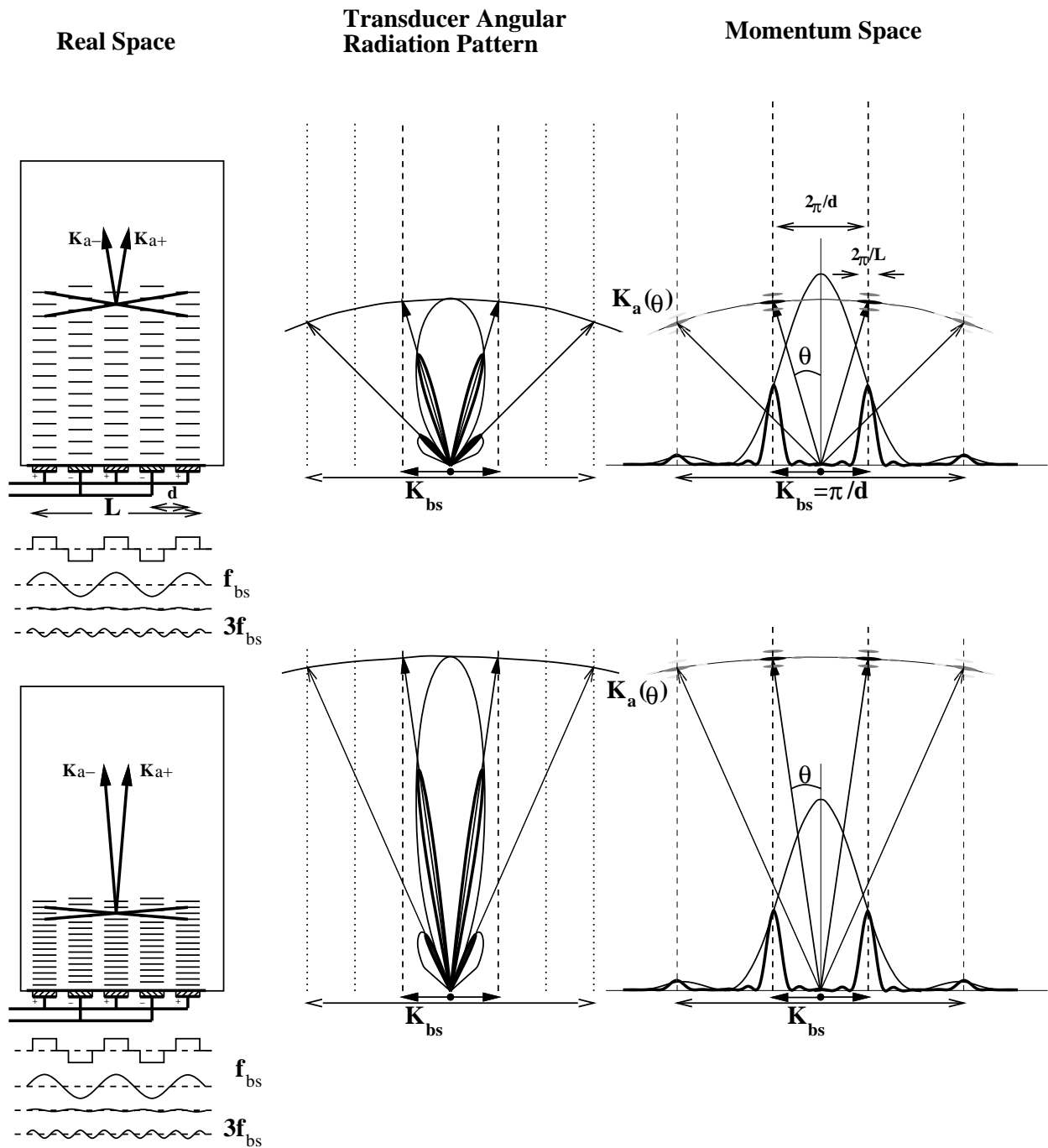


Figure 8: Schematic representation of the dielectric perturbations produced by a phased-array beam-steering transducer at two different frequencies in real space, based on considerations of the transducers angular radiation pattern, and in momentum space.

of acoustic uncertainty traces out straight lines, in this case normal to the transducer face, that has transverse momenta as odd integral multiples of K_{bs} . These considerations lead to the angle of acoustic beam steering as given by $\sin \theta = \frac{|K_{bs}|}{|K_a|} = \frac{2\pi/2d}{2\pi f/v_a(\theta)} = \frac{v_a(\theta)}{2df}$. In normal beam steering acoustooptic deflectors, this locus of beam steering is brought into tangency with the optical momentum surface to obtain wide frequency bandwidth and high efficiency simultaneously.

References

- [1] B. A. Auld, *Acoustic Fields and Waves in Solids*. New York: John Wiley & Sons, 1973.
- [2] J. Sapriel, *Acousto-optics*. John Wiley & Sons, 1979.
- [3] A. Yariv and P. Yeh, *Optical Waves in Crystals*. New York: John Wiley & Sons, 1984.
- [4] A. Korpel, "Acousto-optics," in *Applied Solid State Science* (e. R. Wolfe, ed.), vol. 3, pp. 71–179, New York: Academic Press, 1972.
- [5] D. L. Hecht, "Multifrequency acoustooptic diffraction," *IEEE Transactions on Sonics and Ultrasonics*, vol. SU-24, pp. 7–18, January 1977.
- [6] E. I. Gordon, "A review of acoustooptic deflection and modulation devices," *Proc. IEEE*, vol. 54, no. 10, p. 1391, 1966.
- [7] D. L. Hecht, "Three dimensional acoustooptic dispersion effects in acoustooptic devices for optical information processing," in *Ultrasonics Symposium*, IEEE, 1983.
- [8] I. C. Chang and D. L. Hecht, "Characteristics of acousto-optic devices for signal processors," *Optical Engineering*, vol. 21, pp. 76–81, February 1982.
- [9] A. VanderLugt, "Bragg cell diffraction patterns," *Applied Optics*, vol. 21, pp. 1092–1100, March 1982.

4 Preparation

Read some of the acoustooptic references in the lab

- I. C. Chang, Acousto-optic interactions - a review: I. Acousto-optic devices and applications, *IEEE trans. Sonics and Ultrasonics*, vol. SU-23(1), p. 2 (1976).
- J. Sapriel, *Acousto-optics*, John Wiley & Sons, 1979.
- A. Yariv and P. Yeh, *Optical Waves in Crystals*, John Wiley & Sons, New York, 1984.
- A. Korpel, Acousto-optics, in *Applied Solid State Science*, vol. 3, R. Wolfe, Ed, Academic Press, New York, ch. 2, p. 73 (1972).
- E. I. Gordon, A review of acoustooptic deflection and modulation devices, *Proc. IEEE*, vol. 54(10), p. 1391 (1966).
- I. C. Chang and D. L. Hecht, Characteristics of acousto-optic devices for signal processors, *Opt. Eng.* vol. 21(1), p. 76 (1982).

4.1 Prelab

1. Calculate the internal and external Bragg diffraction angles for an acoustic wave in a cube of fused silica (glass), propagating normal to one of the faces with a velocity of $5.96\text{mm}/\mu\text{sec}$, at a frequency of 100MHz , with an index of 1.46 , illuminated through an orthogonal face by a HeNe laser beam of wavelength of $.6328\ \mu\text{m}$.
2. A fused silica modulator is to be built with an electrode height of 1mm and a length of 5mm , that is designed to operate at $.6328\mu\text{m}$. The diffraction efficiency for this interaction is given by

$$DE = \eta \frac{\sin^2(\eta + (\Delta k L/2)^2)^{1/2}}{\eta + (\Delta k L/2)^2}$$

where Δk is the momentum mismatch, caused by nonoptimal Bragg adjustment for the frequency of operation, L is the transducer length and η is an interaction strength coefficient given by

$$\eta = \frac{\pi^2}{2 \cos^2 \theta} \left(\frac{n^6 p^2}{\rho v_a^3} \right) \frac{P_a L}{H \lambda_0^2} = 5 M_2 P_a \frac{L}{H} \frac{1}{\lambda_0^2}$$

In this expression θ is the Bragg angle and is usually small so the first term is approximately 5 , $n=1.46$ is the index, p is the appropriate photoelastic constant which is about 1 in most materials, $\rho = 2.2\text{g}/\text{cm}^3$ is the density, $v_a = 5.96\text{mm}/\mu\text{sec}$ is the acoustic velocity, P_a is the applied acoustic power, H is the transducer height, L is the interaction length, and λ_0 is the vacuum wavelength. The term in brackets is a figure of merit known as M_2 , which determines the efficiency of a device and ignores bandwidth and power density considerations, and is equal to $1.51 \times 10^{-18} \text{sec}^3/\text{g}$ for fused silica, most other materials are specified relative to this value for fused silica. Calculate the required electrical power necessary to achieve 100% diffraction efficiency assuming a VSWR of $2:1$ (ie contrast ratio of interference between forward and backwards voltage waves $\frac{f+b}{f-b} = 2$ so that $|b|^2 = |f|^2/9$, so that 89% of the electrical power is transformed to acoustic power and the rest is reflected). What is the peak to peak voltage that this corresponds to assuming 50Ω source and load.

3. An acoustic beam steering transducer uses 5 staircase stepped elements with a 20mm spacing, with a step size of $\Delta = \Lambda_c/2 = v_a/2f_c$ in fused silica with $v_a = 6\text{mm}/\mu\text{sec}$ at a center frequency of $f_c=70\text{MHz}$. Calculate the beamsteering angle as a function of frequency between $50\text{-}90\ \text{MHz}$, and calculate the momentum mismatch for the plus and minus diffraction orders in order to derive the bandshape, which is the sinc of the momentum mismatch. Graphical techniques may be used to simplify this problem.

5 Procedure

1. **RF section.** Hook up the HP 8111 pulse generator to the I port of the RF mixer, and the HP RF 8601A oscillator to the L port, and observe the RF output on an oscilloscope and RF spectrum analyzer as you vary the mixer levels and offsets. An RF mixer has three input ports, one for the local oscillator, one for the mixing waveform and one for the IF output, and it should be driven with signals of an appropriate amplitude, typically 10mW or less, have your TA show you how. Set the offset and amplitude on the pulse generator to obtain a clean pulsed RF waveform, with as little modulation in the off time as possible. What is the rise time of the pulse generator, and the modulated RF output? Apply this pulsed RF waveform to the 1W RF amplifier. Make sure the output power is less than 1 Watt peak in order to be sure of not blowing out the piezo-electric transducer . Apply this pulsed RF signal to the acousto-optic modulator that is on a rotation stage.
2. **Bragg alignment.** Spatial filter and collimate the HeNe laser as a 1-2mm pencil beam and align the beam onto the AO modulator aperture. Find the Bragg diffraction by rotating, tilting and translating the AOM. Optimize the diffraction efficiency visually, by looking at a card placed 10-30cm beyond the AOM as you vary the alignment and identify the diffracted spot or spots. Often a good starting place for this alignment procedure is to come in at normal incidence with the HeNe, so that numerous diffraction orders are generated, both plus and minus, then to rotate to maximize the +1 order and suppress all of the others. Sketch your setup and the output plane, showing why this is the +1 order, and not the -1 order. Now rotate the AOM to produce primarily the -1 order and sketch your setup.
3. **Acousto-optic modulation.** Block the undiffracted beam and place the power meter in the diffracted beam; measure the diffraction efficiency as a function of applied RF power which is controlled by varying the pulse amplitude. Plot your results, remember to correct for the duty cycle of the RF pulses. Now place a high speed photodetector in the diffracted beam, and observe the detected output on an oscilloscope. Re-optimize the diffraction and measure the diffraction efficiency by detecting both the diffracted and undiffracted waveforms, looking for depletion of the undiffracted beam. Make sure that you are not saturating your detector. What is the rise time that you were able to obtain with this configuration. This is **not** the proper way to operate an acousto-optic modulator for high speed modulation, but it will work for low speed applications.
4. **Access time-diffraction efficiency trade-off.** Re-collimate the laser beam with a 5-10mm diameter, place an iris in the beam, and place a lens beyond the aperture and one focal length before the modulator so you are focusing to a tiny spot in the center of the AOM. Realign angle and position to maximize the diffraction efficiency, paying attention to the vertical alignment of the spot with the acoustic column. Now observe a far-field output plane as you open and close the aperture. Sketch and describe your observations. Is the diffracted output spot well separated from the undiffracted spot? Is the diffracted spot always circular, or does it change its shape for very wide apertures? The optimal setting for the aperture, in the sense of efficiency-rise time trade-off, is the largest aperture at which the full beam is diffracted, and phase matching selectivity has not become overly constraining. Place a high speed photodetector in the diffracted beam, and open the aperture so that the diffracted and undiffracted beams overlap. How can you verify that the diffracted beam is Doppler shifted due to the acoustic motion, and what is that Doppler shift? Now with

the aperture smaller so the beams don't overlap, measure the rise time and peak diffraction efficiency (not diffracted power, but ratio of diffracted output to input) as a function focal spot size, varied inversely $\Delta = \lambda F/A$ by opening and closing the aperture A (or perhaps by z-shifting the AOD). Note the RF power levels. Do not confuse total power with diffraction efficiency, since you are varying the total power as you open and close the aperture. Another way to determine the diffraction efficiency is to look at the depth of the hole dug in the undiffracted light as the acoustic pulse scrolls through the focal spot. Plot your results of rise time and diffraction efficiency as a function of the spot size in the crystal. What is the optimal spot size and aperture setting in the sense of maintaining high diffraction efficiency and minimum rise time? Compare the optimum aperture size obtained from your plot and that obtained by the phase matching method. Realign an imaging system to image the pinhole onto the AOD producing the same spot size without an aperture, so that the cone angle is the same as the optimized AOM. You now have an optimally aligned AOM.

5. **Acoustooptic deflector, or Bragg cell.** Replace your acoustooptic modulator with the acoustooptic deflector and illuminate with a wide aperture collimated plane wave from a 2" lens. Apply an RF signal from the HP 8601A directly to the AOD, which is in the range from 50-110 MHz, and with an amplitude of less than 1 Watt. Use a 2 inch diameter 500mm focal length lens to Fourier transform the output of the AO deflector, and observe the Fourier plane as you rotate the device around a vertical axis in the Bragg plane. When the acoustooptic device is normal to the incident laser beam you should see symmetric orders on both sides of the undiffracted beam corresponding to the positive and negative diffracted orders. Which is which? When you rotate the device away from this position you should be able to optimize the diffraction efficiency into either of the diffracted orders. However, because this Bragg cell uses a stepped staircase acoustic beam-steering transducer, the bandwidths of the two orders will be entirely different. Put the signal generator in broadband sweep mode, and watch the diffracted spot move across the Fourier plane. Observe the bandwidth of the two orders by watching the width or time that the diffracted light scans across the Fourier plane. Use the sweep ramp output as the x input to the oscilloscope, and place a wide area photodetector (such as the power meter) in the diffracted beam, and use the photodetector output as the y input to the oscilloscope (watch out for power-meter auto-ranging). With the oscilloscope placed in x-y mode the pattern displayed is the acoustooptic band-shape function. Measure the band shape of the plus and minus orders and photograph, and notice that the band shape for either of the orders varies as you rotate the AO cell. The envelope of these AO band-shape curves is the acousto-electric band shape of the piezo-electric transducer. Rotate the cell to the mid band of the order that gives the widest bandwidth and largest diffraction efficiency.
6. **Acoustooptic Spectrum Analyzer.** Place the line scan CCD array in the Fourier plane, where it will intercept the diffracted order from the AOD. Apply the required power to the CCD and observe the CCD output on the oscilloscope. Align the array for best focus and maximum detected power across the full AOD bandwidth. Observe the CCD output as you slowly scan the input frequency across the AOD bandwidth. Calibrate the detected location with the applied frequency. What is the frequency increment per pixel as the spot moves across the array, and what is the obtainable resolution of this acoustooptic spectrum analyzer system. Apply a pulsed RF waveform to the AOD, which is produced by mixing a pulse train produced by the HP8111 with an RF carrier produced by the HP8601A using an RF mixer,

and observe the detected spectra. From this spectra and your calibration measurements, calculate the modulator center frequency and pulse width, and compare with your other measurements of these parameters. Vary the pulse width and pulse repetition frequency and observe the effects on the detected spectra, and change to a sinusoidal waveform and observe the result on the CCD.

7. **Heterodyne detection. (Extra Credit)** Use a beam splitter inserted before the AOD to split off a plane wave reference beam, and recombine this co-linearly with the diffracted beam at the Fourier plane using another beam splitter in a Mach-Zehnder interferometer configuration. Place a high speed photodetector in this interference plane as you apply a single frequency from the HP8601A to the AOD, and observe the detector output. You should be able to see an interferometric reconstruction of the signal applied to the AOD, as long as the diffracted spot is hitting the detector, the reference beam is co-linear, and the detector is fast enough. Block the reference beam and describe the change in the output. As you change the frequency from the signal generator what happens to the output. Place a small opaque object such as a resistor wire in front of part of the detector as a band-pass filter, and describe the detected waveform as you sweep the diffracted light across the detectors face.
8. **Time integrating correlator.(Extra Credit)** Place the AOM in the unexpanded laser beam before the Bragg cell, and align the system so that the diffracted beam produced by the AOM is re-diffracted by the AOD. Alternatively the AOM can go in the reference arm of the heterodyne interferometer. Image the diffracted beam from the AOD onto the time integrating CCD detector array, and block all undiffracted beams. Set up the HP8111 pulse generator to produce a pulse train of 200ns pulses at a rate of 1MHz, and use this as the external AM modulation to the HP8601A sweep generator, setup to produce a single tone. Apply this signal to both the AOM and the AOD and observe the time integrated correlation on the CCD output. You need to make sure that the acoustic time delay is equal to the modulation spot in the AOM and some position within the illuminated AOD aperture. Vary the PRF and duty factor of the pulse train and describe your results. Use a chirp waveform for even better results.